In vivo Real-time Tracking of Single Quantum Dots Conjugated with Monoclonal Anti-HER2 Antibody in Tumors of Mice

Hiroshi Tada,[1] Hideo Higuchi,[2] Tomonobu M. Wanatabe,[2] and Noriaki Ohuchi[1]

[1]Division of Surgical Oncology, Graduate School of Medicine and [2]Biomedical Engineering Research, Organization, Tohoku University, Sendai, Japan

Abstract

Studies with tracking of single nanoparticles are providing new insights into the interactions and processes involved in the transport of drug carriers in living mice. Here, we report the tracking of a single particle quantum dot (Qdot) conjugated with tumor-targeting antibody in tumors of living mice using a dorsal skinfold chamber and a high-speed confocal microscope with a high-sensitivity camera. Qdot labeled with the monoclonal anti-HER2 antibody was injected into mice with HER2-overexpressing breast cancer to analyze the molecular processes of its mechanistic delivery to the tumor. Movement of single complexes of the Qdot-antibody could be clearly observed at 30 frames/s inside the tumor through a dorsal skinfold chamber. We successfully identified six processes of delivery: initially in the circulation within a blood vessel, during extravasation, in the extracelullar region, binding to HER2 on the cell membrane, moving from the cell membrane to the perinuclear region, and in the perinuclear region. The six processes were quantitatively analyzed to understand the rate-limiting constraints on Qdot-antibody delivery. The movement of the complexes at each stage was "stop-and-go." The image analysis of the delivery processes of single particles *in vivo* provides valuable information on antibody-conjugated therapeutic nanoparticles, which will be useful in increasing therapeutic efficacy. [Cancer Res 2007;67(3):1138–44]

Introduction

Recent anticancer therapeutics based on active tumor targeting by conjugating tumor-specific antibodies has become of great interest in oncology, pharmacology, and nanomedicine. This approach will allow to increase therapeutic efficacy and to decrease systemic toxicity (1–3). Quantitative investigation of the dynamics of such delivery *in vivo* is crucial in enabling the development of more effective drug delivery systems. One of the best ways to do this is to apply a new technology in biophysics wherein the positions of proteins are detected quantitatively at the single molecule or particle level with nanometer precision (4). However, the specific processes of its delivery *in vivo* postinjection are not known at the single particle level. Conventional modalities of *in vivo* imaging such as computed tomography, magnetic resonance imaging, positron emission tomography, and organic fluorescence or luminescence imaging have insufficient resolution to analyze the pharmacokinetics of drugs at the single particle level *in vivo* (5).

To address the issue, real-time single particle tracking using quantum dots (Qdots) has been applied to the study of drug delivery. Qdots, fluorescence nanocrystals, were thought to be as a suitable marker because of their intense brightness and stability, in contrast to organic dyes and green fluorescent protein (6–8). In cultured cells, single particle tracking has yielded invaluable information on the function of purified proteins (9–11). Recent work shows that the antibody-conjugated Qdots have allowed real-time tracking of single receptor molecules on the surface of live cells (12). However, no real-time single particle tracking in live animals has been reported, and it is uncertain that single particles of Qdots could be observed and tracked in live animals. The analysis of single molecules and particles in living animals is crucial to the understanding of the molecular mechanism of proteins *in vivo*.

This study was designed to analyze the movement of single functional Qdots in tumors of mice from a capillary vessel to cancer cells. To observe single Qdot particles in tumor tissue, we used a dorsal skinfold chamber model (13) and a high-resolution intravital imaging system. The imaging system, which consists of a confocal scanner unit with a Nipkow type disk and an electron multiplying charge coupled device (EMCCD) camera (14), facilitates the high-resolution *in vivo* single particle tracking at a video rate with a high spatial resolution of 30 nm. In addition, quantitative and qualitative information such as velocity, directionality, and transport mode was obtained using time-resolved trajectories of particles. As a result, we successfully identified the processes of delivery; these were quantitatively analyzed to understand the rate-limiting constraints on single Qdot-antibody delivery *in vivo*.

Materials and Methods

Qdot-antibody conjugation. Qdot was conjugated to trastuzumab (Herceptin, Chugai Pharmaceuticals Co., Ltd., Tokyo, Japan) with a Qdot 800 Antibody Conjugation Kit (Quantum Dot Corp., Hayward, CA) coated with polyethylene glycol (PEG) amine (MW 2,000) according to the manufacturer's instruction. Briefly, Qdots are activated with the heterobifunctional cross-linker 4-(maleimidomethyl)-1-cyclohexanecarboxylic acid *N*-hydroxysuccinimide ester (SMCC), yielding a maleimide-nanocrystal surface. Excess SMCC is removed by size exclusion chromatography. Antibody is then reduced and fragmented by DTT to expose free sulfhydryls, and excess DTT is removed by size exclusion chromatography. Then, activated Qdots are covalently coupled with reduced antibody and reaction is quenched with β-mercaptoethanol. The molar ratio of trastuzumab fragments to the Qdots at mixing is ~3:1. Conjugates are concentrated by ultrafiltration and purified by size exclusion chromatography. This active ester maleimide–mediated amine and sulfhydryl coupling (by SMCC) is a popular cross-linking reaction for various antibody conjugations. After this reduction,

Note: Supplementary data for this article are available at Cancer Research Online (http://cancerres.aacrjournals.org/).

Requests for reprints: Hideo Higuchi, Biomedical Engineering Research Organization, Tohoku University, Engineering research Lab complex, 6-6-11 Aramaki, Aoba-ku, Sendai, Miyagi 980-8578, Japan. Phone: 81-22-795-4735; Fax: 81-22-795-5753; E-mail: higuchi@tubero.tohoku.ac.jp.

doi:10.1158/0008-5472.CAN-06-1185

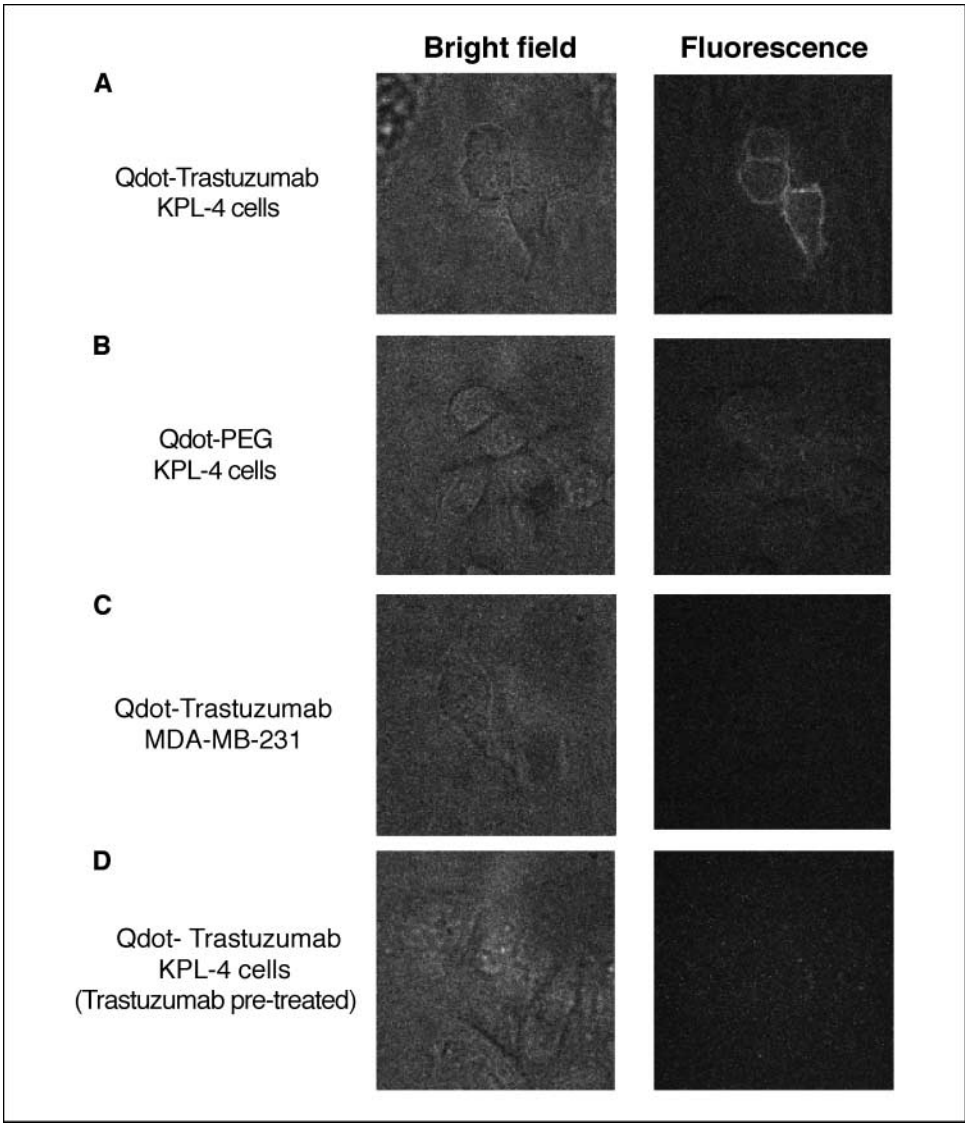

Figure 1. Immunocytochemical studies of QT-complex binding activity in cultured breast cancer cells. *A,* KPL-4 cells, which are HER2 positive, as revealed by the presence of the QT complex on the cell surface. *B,* negative staining was detected in KPL-4 cells exposed to QD-PEG in the absence of anti-HER2 antibody. *C,* negative staining was detected in MDA-MB-231 cells, which are HER2 negative. *D,* competition study of QT complex and trastuzumab. After addition of 100 nmol/L trastuzumab to KPL-4 cells, QT-complex fluorescence was absent. QT-complex fluorescence was detected on the cell surface of KPL-4 but not MDA-MB-231, confirming HER2 as a cell surface–specific marker for some breast cancer cell lines.

it has been found to have little or no effect on their binding ability. QT complex [Qdot (Q)-trastuzumab (T) complex] was fractionated by agarose gel electrophoresis into three major bands. Approximately 60% of the QT complex was conjugated with three antibody fragments, ~30% with two fragments, and ~10% with a single fragment (data not shown).

The final concentration of QT complexes was determined by measuring the conjugate absorbance at 550 nm and using an extinction coefficient of 1,700,000 M^{-1} cm^{-1} at 550 nm.

Cell line and mouse model. The human breast cancer cell line KPL-4, which overexpresses HER2 and is sensitive to trastuzumab (15, 16), was kindly provided by Dr. J. Kurebayashi (Kawasaki Medical school, Kurashiki, Japan). KPL-4 cells were cultured in DMEM supplemented with 5% fetal bovine serum (FBS). MDA-MB-231 cells were maintained in RPMI with 10% FBS. Conventional immunohistochemical procedures were used to determine the binding of QT-complex conjugate to KPL-4 cells, using both QD-PEG (no antibody) and MDA-MB-231 as negative controls. In these studies, QT-complex or QD-PEG bioconjugates (100 nmol/L) were incubated with the cells for 30 min at 37°C, washed, and photographed. For competition study of QT complex and trastuzumab, KPL-4 was pretreated with trastuzumab (100 nmol/L) for 30 min before exposure to 100 nmol/L QT complex.

A suspension of KPL-4 cells (0.8×10^7 per mouse) was transplanted s.c. to the dorsal skin of female BALB/c *nu/nu* mice at 6 to 10 weeks of age (Charles River Japan, Yokohama, Japan). Several weeks after tumor inoculation, mice bearing a tumor volume of 100 to 200 mm^3 were selected. All of the mice were maintained in our pathogen-free institutional facilities. All operations on animals were in accordance with the institutional animal use and care regulations.

QT complexes were injected into the tail vein of mice at a concentration of 2 μmol/L and a volume of 100 μL. The mice were placed under anesthesia by the i.p. injection of a ketamine and xylazine mixture at dosages of 95 and 5 mg/kg, respectively. The temperature of mice was maintained at 37°C with a thermoplate and objective lens heater.

The dorsal skinfold chamber, previously described (13) and modified for this study, was used to fix the exposed mouse tumor on the stage of the microscope. Two sterilized polyvinyl chloride plates (0.5-mm thickness) containing a window were mounted to fix the extended double layer of dorsal skin including the tumor site. Skin between chambers was sutured together with 6-0 nylon around the window so the tumor could be located in the center of the window and fixed without influence from the beating of the heart and/or breathing. The tumor was exposed by oval incision of ~10-mm diameter, and the s.c. connective tissue was removed. The tumor was then placed surface down in neutral saline, mounted on coverslip, and viewed under an inverted microscope. The mouse was fixed to a metal plate on the stage designed to stabilize the chamber. Tumors can be visualized directly by means of this setup.

After imaging, the mice were sacrificed by CO_2 overdose. The tumors were removed and divided for histologic Qdot uptake study and immunohistochemical analysis. For the histologic Qdot uptake study, tumors were frozen and cryosectioned (6-μm thickness), fixed with acetone at 0°C, and examined with an imaging system. For immunohistologic examination, tumors were fixed in 10% neutral-buffered formalin overnight and then transferred to ethanol before processing and paraffin embedding. Immunohistochemical analysis was done on paraffin sections of 6-mm thickness using the HercepTest (DakoCytomation, Carpinteria, CA).

***In vivo* imaging and tracking.** *Optics and image analysis:* The optics system for three-dimensional observation consisted primarily of an epifluorescent microscope (IX71, Olympus, Tokyo, Japan) with modifications (17, 18), a Nipkow lens type confocal unit (CSU10, Yokokawa, Japan), and an electron multiplier type CCD camera (iXon 887, Andor, Tokyo, Japan). The confocal unit adopts multibeam scanning using about a thousand beams that are simultaneously emitted through a pin-hole disk to facilitate high-speed scanning. The EMCCD has an advantage that offers unsurpassed sensitivity performance and has been shown to yield markedly improved S/N (signal/noise) ratio (14). The object lens (60×, numerical aperture 1.45) was moved by a piezo actuator with a feedback loop (Nanocontrol) for stabilizing the position of the focus. A computer controlled the piezo actuator in synchronization with the image acquisitions that the object lens remained within the exposure time of the CCD camera. An area of $\sim 30 \times 30\ \mu m^2$ was illuminated by a green laser (532 nm, CrystaLaser, Reno, NV). This system captures images of single Qdot at a video rate of 33 ms/frame. Three-dimensional confocal intravital images of single QT complex were taken by moving an objective lens (Fig. 2*A*). Three-dimensional images of the tumor were taken by reconstructing 10 to 20 confocal images from the surface of the mice to a depth of 150 μm inside the tumor through the DSFC.

The *xy* position of the fluorescent spot was calculated by fitting to a two-dimensional Gaussian curve. The single molecule could be identified by the fluorescence intensity. In addition, quantitative and qualitative information such as velocity, directionality, and transport mode was obtained using time-resolved trajectories of particles. The resolution of the position was determined from the position of immobile QT complexes in a chemically fixed tumor cell. The resolution of the *x* and *y* directions of images taken at an exposure time of 33 ms was 30 nm, taking into consideration the SD.

Results and Discussions

***In vitro* study.** Qdots were conjugated to trastuzumab using the Qdot-antibody conjugation kit (QT complex). Immunocytochemical data confirmed strong and specific binding of the QT complex to a HER2-overexpressing human breast cancer cell line (Fig. 1*A*). QD-PEG without antibody showed almost no binding to KPL-4 cells (Fig. 1*B*). MDA-MB-231, a HER2 negative human breast cancer cell line, showed the absence of Qdot binding (Fig. 1*C*). KPL-4 cells pretreated by excess trastuzumab also showed the absence of Qdot binding (Fig. 1*D*). These results indicate that QT complexes selectively bind to the HER2 protein. Furthermore, QT complex was compared with trastuzumab labeled with rhodamine, which is recognized as similar to native trastuzumab. Both QT complex and rhodamine-trastuzumab bound to the KPL-4 cell at concentrations of 1 nmol/L but hardly at 0.1 nmol/L, indicating the binding properties of QT complex are similar to those of native antibody (data not shown).

Three-dimensional imaging of single Qdot-trastuzumab in mice. It is reported that the accumulation of trastuzumab at the HER2-overexpressing tumor site in mice model is the basis for radioimmunoscintigraphic scanning and targeted therapy for human HER2-overexpressing breast cancer (19–21). Here tumor-bearing mouse models were prepared with KPL-4 s.c. implantation. The QT complex accumulated in the tumor specifically because only the tumor area generated fluorescence of Qdots (Supplementary Fig. S1*A* and *B*). Single Qdots in the mice tumor were observed using a high-resolution intravital imaging system through the dorsal skinfold chamber (Fig. 2*A*; ref. 13). Fluorescence microangiography was done after injection of the QT complexes into the tail vein. After injection, blood sample from mice was examined by fluorescence observation on whether QT complex had made the aggregation in the mice. QT complex existed as a single particle without further aggregation (data not shown). The membranes of the KPL-4 tumor cells were clearly stained with single QT complexes at 6 h after the injection. At 24 h after the injection, the QT complexes had been internalized into the tumor cells (Fig. 2*B* and *C*). After imaging of the tumors in the living mice, histologic examination of the chemically fixed tumors was done to confirm that QT complexes in the living mice exhibit activity in KPL-4 cells. QT complexes observed under a three-dimensional microscope were located at the cell membrane and near the nuclear membrane (Supplementary Fig. S2*A* and *B*). An adjacent slice of the observed area was further stained

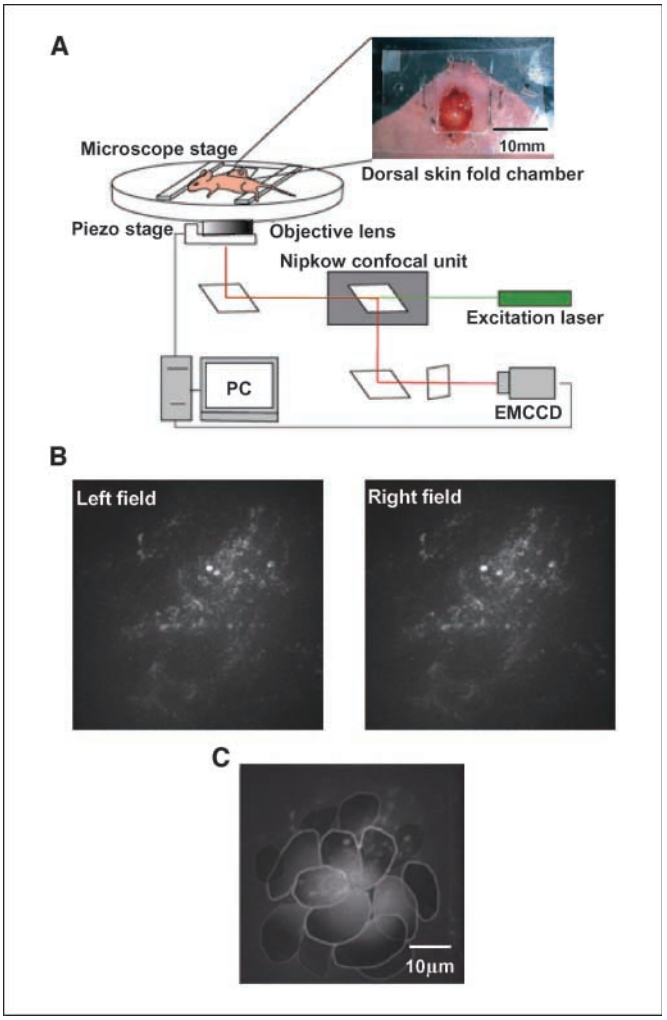

Figure 2. Experimental diagram and three-dimensional intravital cancer imaging. Mice prepared for dorsal skinfold chamber were fixed on the microscopic stage. QT complexes were injected into the tail vein of nude BALB/c mice bearing KPL-4 breast cancer xenograft tumor. *A,* three-dimensional microscopic system consisting of a confocal unit, an EMCCD, and a computer to control the piezo stage. *B,* three-dimensional image of the tumor was obtained by the QT complexes binding to tumor cell membrane (stereoscopic image: left and right field). *C,* traced outlines of the cells shown in (*B*).

immunohistochemically with the anti-HER2 antibody A0485. The cell membrane stained locally in the adjacent slice (Supplementary Fig. S2*C*), confirming that QT complexes were present on the membrane of tumor cells.

Extravasation of single QT complexes in tumors of mice with two-dimensional imaging. After the injection, three-dimensional images of the tumor were taken to allow observation on the tumor vessel of single QT complexes. The position of the objective was fixed and 300 to 3,000 sequential confocal two-dimensional images (total, 10–100 s) were taken at this fixed position. Within 30 s after the injection, the current of the QT complex in a vessel was observed. When the vessel and cells were clearly observable, the the current of single QT complex in the tumor vessel was then analyzed. The fluorescent image of the circulating QT complex was not a circle but an ellipse and sometimes a line at the video rate because QT complex at times moved >1 μm in single frame. The speed of the movement of the single particles was calculated from the positional changes of the centroid of the QT complex images (Fig. 3*A*). The average speed of each complex ranged from 100 to 600 μm/s, in agreement with a previous report by another method (22). As shown in Fig. 3*A*, each particle exhibits slow and fast movement in the bloodstream. Such fast and slow movement characteristics could be induced by the pulse and nonuniform current within a vessel such as the Hagen-Poiseuille current. The slow speed of the complexes inside a tumor vessel would be important to locate pores between the vessel cells and then the complexes diffuse out from these pores.

Focusing on the vessel walls, a movement was observed of the complex extravasated from the intravascular space (Fig. 3*B*). The edge of the vascular inner surface was not clear on a single frame image. Therefore, all the images obtained were averaged to precisely determine the position of the edge (Fig. 3*B, i–iii*). The complexes were positioned first on the vascular surface and then extravasated. This is the first example of video rate observation of extravasation of very small particles, such as Qdots, in a mouse model. The moving speed of the complexes was very low, 1 to 4 μm/s, at the pore of the vascular cells, compared with the speed in the current. The QT complexes either interacted with the vascular cells or became trapped in the extracellular matrix.

Diffusion of single QT complexes in extracellular and intercellular regions. Two hours after the injection, many complexes had migrated into the tumor interstitial area close to the tumor vessels. Most of the movement of the complexes was random in orientation and speed, indicating that complexes diffuse by the Brownian motion exerted by thermal energy. The average diffusion coefficient of the complexes was 0.0014 $\mu m^2/s$, much smaller than that at free diffusion in solution ($\sim 10\ \mu m^2/s$). Many complexes also moved randomly within a restricted small area of $\sim$1-μm diameter and then hopped by $\sim$1 μm (Fig. 4*A*). These results indicate that movement is restricted by a cage formed by the extracellular matrix and, at times, complexes escape from this cage.

Binding of QT complexes to cell membrane and vesicle transport. Six hours after the injection, QT complexes had bound to the KPL-4 cell membrane on which the HER2 protein is located. We successfully captured specific images of the QT complexes bound to the cell membrane (Fig. 4*B*). Movements of single QT complex are identified in single frames. To identify the positions of the tumor vessels and cells in living mice without further fluorescence staining, images were averaged (Supplementary Fig. S3*A*). As viewed from the outside of the delineated cells, the QT complexes moved toward the cell membrane at a speed of 200 to 400 nm/s (Fig. 4*C*), remained on the membrane for a few seconds, and then moved randomly along the membrane. QT complexes moved between the cells, bound to HER2, and then moved in association with HER2 on the membrane.

Many QT complexes bound to the cell membrane exhibited Brownian motion within a restricted region of $\sim$500-nm diameter. The region is significantly larger than the area of $\sim$30 nm, which was drawn by position noise of the complexes fixed on a coverslip, indicating the movement is due to the anchor of the HER2 to a flexible component of the cytoskeleton such as an actin filament (23). The QT complexes restricted to the small area initiated linear movement in one direction along the cell membrane with a speed of 400 to 600 nm/s and traveled for several micrometers (Fig. 5*A* and *B*; Supplementary Fig. S3*B*).

We also succeeded in pursuing the transport of QT complexes from the peripheral region of the cell to the perinuclear region

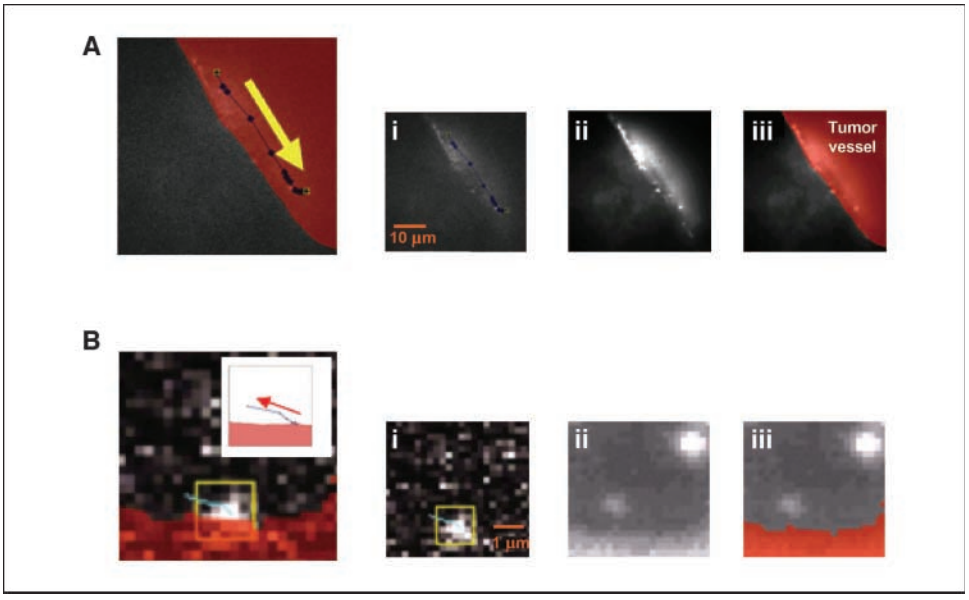

Figure 3. The movement of QT complexes from tumor vessels to the interstitial space. *A,* flow of QT complexes in the tumor vessel. The speed was calculated by the moving distance per 33 ms. The maximum speed was $\sim$600 μm/s. *B,* extravasation of QT complexes from the vascular space of the tumor. *Dotted line,* trajectory of the extravasation. *i,* an initial single frame tracing the trajectory of a single QT complex shown as a dotted line at video rate. *ii,* sequential frames were averaged to define the edge of vessel. *iii,* tracing of the outlines of tumor vessels. Overlapping initial single image and (*iii*), the tracing image gives the final images. *B, inset,* magnified image of the trajectory of extravasating QT complex.

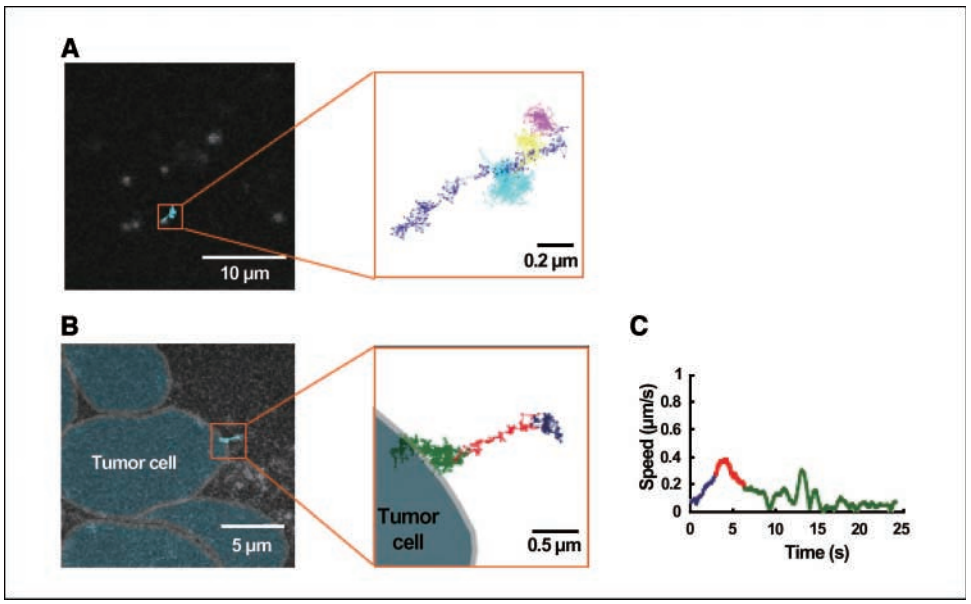

Figure 4. Tracking the movement of QT complexes from the interstitial space to the cell membrane. *A,* trajectory of the QT complexes in the interstitial space near the tumor vessels and magnified trajectory. The color of the trajectory codes the time axis from black to pink, yellow, and light blue. *B,* trajectory of the binding to the cell membrane and magnified trajectory. *C,* time trajectory of the velocity of (*B*). The color of the trajectory of both (*B*) and (*C*) codes the time axis from blue to red and green. All time trajectories of the velocity are calculated by the least squares method (2 s).

(Fig. 5*C*; Supplementary Fig. S3*C*). The QT complex in a given cell moved almost straight toward the cell membrane with a velocity of 100 to 300 nm/s, changed direction to parallel to the cell membrane, and moved toward the cell nucleus at a velocity of ~600 nm/s (Fig. 5*D*). Finally, the directional movement of the QT complexes ceased and Brownian motion commenced within a small area, ~1 μm in a diameter, near the nucleus (Fig. 5*C* and *D, black line*). The first two movements of straight toward and along the cell membrane would most likely be produced by the transport of an acto-myosin system binding to vesicle containing QT complexes (24, 25). Because the actin filaments in cultured cells are highly concentrated in the peripheral region of cells, movement toward the nucleus would most likely be on a microtubule transported by dynein (26) as there are almost no actin filaments near nucleus, but rather, a high concentration of microtubules.

Summary of the delivery processes. We have succeeded in capturing the specific delivery of single QT complexes in tumor vessels to the perinuclear region of tumor cells in live mice after QT complexes had been injected into the tail vein of mice. Six stages were detected (Fig. 6): (*a*) vessel circulation, (*b*) extravasation, (*c*) movement into the extracellular region, (*d*) binding to HER2 on the cell membrane, (*e*) movement from the cell membrane to the perinuclear region after endocytosis, and (*f*) in the perinuclear region. The translational speed of QT complexes in each process was highly variable, even in the vessel circulation. The movement of the complexes in each process was also found to be "stop-and-go" (i.e., the complex remaining within a highly restricted area and then moving suddenly). This indicates that the movement was promoted by a motive power and constrained by both the three-dimensional structure and protein-protein interactions. The motive

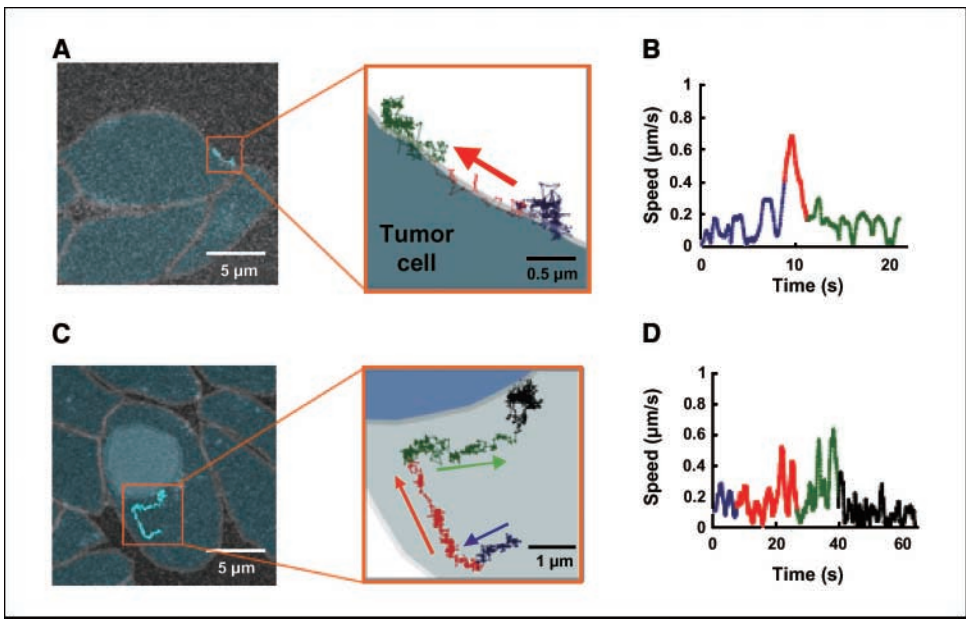

Figure 5. Tracking of the movement of QT complexes from the cell membrane to the perinuclear region. *A,* trajectory of the QT complexes binding to the cell membrane and magnified image. *B,* time trajectory of the velocity of (*A*). The color of the trajectory of both (*A*) and (*B*) codes the time axis from blue to red and green. *C,* trajectory of the intracellular transport of QT complex and magnified image. *D,* time trajectory of the velocity of (*C*). The color of the trajectory of both (*C*) and (*D*) codes the time axis from blue to red, green, and black. All time trajectories of the velocity are calculated by the least squares method (2 s).

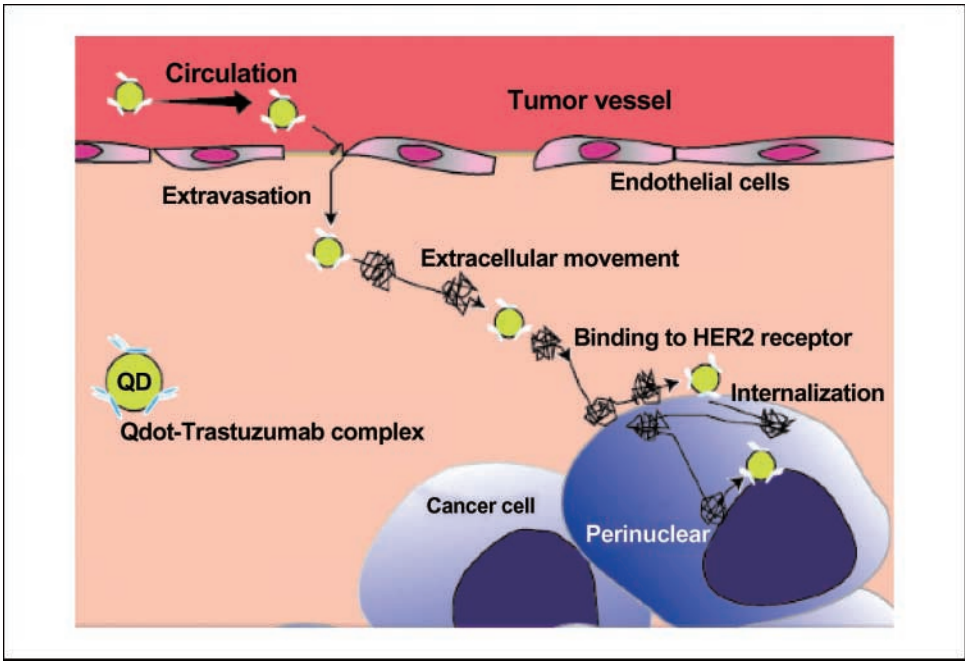

Figure 6. Schematic illustration of the QT complex, the QT complex entered into the circulation, extravasated into the interstitial space from the vascular space, bound to the tumor cells through the interstitial region, and having reached the perinuclear region after traveling on the intracellular rail protein. All processes exhibit a characteristic "stop-and-go" movement.

power of the movements was produced by blood circulation (essential in processes *a* and *b*), diffusion force driven by thermal energy (*b, c*, and *d*), and active transport by motor proteins (*e*). The cessation of movement is most likely induced by a structural barricade such as a matrix cage (*b, c*, and *f*) and/or specific interaction between proteins (e.g., an antibody) and HER2 (*d*), motor proteins, and rail filaments such as actin filaments and microtubules (*e*).

The molecular mechanism underlying the movement and its cessation during delivery of nanoparticles in animal models is the fundamental basis of drug delivery. There have been many different approaches to tumor-targeting "nanocarriers" including anticancer drugs for passive targeting, such as Myocet (27) and Doxil (28), and for active targeting, such as MCC-465 (29) and anti-HER2 immunoliposome (19). There is still very little understanding of the biological behavior of nanocarriers, including such crucial features as their transport in the blood circulation, cellular recognition, translocation into the cytoplasm, and final fate in the target cell. These results suggest that the transport of nanocarriers would be quantitatively analyzable in the tumors of living animals by the present method. This approach should thus afford a potential new insight into particle behavior in complex biological environments. Such new insight in turn will allow rational improvements in particle design to increase the therapeutic index of the tumor-targeting nanocarriers.

Acknowledgments

Received 4/4/2006; revised 8/24/2006; accepted 12/5/2006.

Grant support: Grants-in-aid for Research Project; Promotion of Advanced Medical Technology (H14-Nano-010, H18-Nano-General-001); Ministry of Health, Labor, and Welfare of Japan (N. Ohuchi); Scientific Research in Priority Areas from the Japan MEXT and CREST from the JST (H. Higuchi); and Special Coordination Funds for Promoting Science and Technology of Japan (H. Higuchi and T.M. Wanatabe).

The costs of publication of this article were defrayed in part by the payment of page charges. This article must therefore be hereby marked *advertisement* in accordance with 18 U.S.C. Section 1734 solely to indicate this fact.

We thank Dr. H.A. Nguyen for helpful discussion and Dr. J.M. West for critical reading of the manuscript.

References

1. Mamot C, Drummond DC, Noble CO, et al. Epidermal growth factor receptor-targeted immunoliposomes significantly enhance the efficacy of multiple anticancer drugs *in vivo*. Cancer Res 2005;65:11631–8.
2. Torchilin VP, Lukyanov AN, Gao Z, Papahadjopoulos-Sternberg B. Immunomicelles: targeted pharmaceutical carriers for poorly soluble drugs. Proc Natl Acad Sci U S A 2003;100:6039–44.
3. Krauss WC, Park JW, Kirpotin DB, Hong K, Benz CC. Emerging antibody-based HER2 (ErbB-2/neu) therapeutics. Breast Dis 2000;11:113–24.
4. Ishijima A, Kojima H, Funatsu T, et al. Simultaneous observation of individual ATPase and mechanical events by a single myosin molecule during interaction with actin. Cell 1998;92:161–71.
5. Lyons SK. Advances in imaging mouse tumour models *in vivo*. J Pathol 2005;205:194–205.
6. Wu X, Liu H, Liu J, et al. Immunofluorescent labeling of cancer marker Her2 and other cellular targets with semiconductor quantum dots. Nat Biotechnol 2003;21:41–6.
7. Bruchez M, Jr., Moronne M, Gin P, Weiss S, Alivisatos AP. Semiconductor nanocrystals as fluorescent biological labels. Science 1998;281:2013–6.
8. Gao X, Cui Y, Levenson RM, Chung LW, Nie S. *In vivo* cancer targeting and imaging with semiconductor quantum dots. Nat Biotechnol 2004;22:969–76.
9. Endow SA, Higuchi H. A mutant of the motor protein kinesin that moves in both directions on microtubules. Nature 2000;406:913–6.
10. Yildiz A, Forkey JN, McKinney SA, Ha T, Goldman YE, Selvin PR. Myosin V walks hand-over-hand: single fluorophore imaging with 1.5-nm localization. Science 2003;300:2061–5.
11. Dahan M, Levi S, Luccardini C, Rostaing P, Riveau B, Triller A. Diffusion dynamics of glycine receptors revealed by single-quantum dot tracking. Science 2003;302:442–5.
12. Lidke DS, Nagy P, Heintzmann R, et al. Quantum dot ligands provide new insights into erbB/HER receptor-mediated signal transduction. Nat Biotechnol 2004;22:198–203.
13. Leunig M, Yuan F, Menger MD, et al. Angiogenesis, microvascular architecture, microhemodynamics, and interstitial fluid pressure during early growth of human adenocarcinoma LS174T in SCID mice. Cancer Res 1992;52:6553–60.
14. Chong FK, Coates CG, Denvir DJ, McHale NG, Thornvury KD, Hollywood MK. Optimization of spinning disk confocal microscopy: synchronization with the ultra-sensitive EMCCD. Proc SPIE 2004;5324:65–76.
15. Kurebayashi J, Otsuki T, Tang CK, et al. Isolation and characterization of a new human breast cancer cell line, KPL-4, expressing the Erb B family receptors and interleukin-6. Br J Cancer 1999;79:707–17.

16. Fujimoto-Ouchi K, Sekiguchi F, Tanaka Y. Antitumor activity of combinations of anti-HER-2 antibody trastuzumab and oral fluoropyrimidines capecitabine/5′-dFUrd in human breast cancer models. Cancer Chemother Pharmacol 2002;49:211–6.
17. Nguyen VT, Kamio Y, Higuchi H. Single-molecule imaging of cooperative assembly of γ-hemolysin on erythrocyte membranes. EMBO J 2003;22:4968–79.
18. Nguyen H, Higuchi H. Motility of myosin V regulated by the dissociation of single calmodulin. Nat Struct Mol Biol 2005;12:127–32.
19. Park JW, Kirpotin DB, Hong K, et al. Tumor targeting using anti-her2 immunoliposomes. J Control Release 2001;74:95–113.
20. Ballangrud AM, Yang WH, Palm S, et al. α-Particle emitting atomic generator (Actinium-225)-labeled trastuzumab (Herceptin) targeting of breast cancer spheroids: efficacy versus HER2/neu expression. Clin Cancer Res 2004;10:4489–97.
21. Wiercioch R, Balcerczak E, Byszewska E, Mirowski M. Uptake of radiolabelled Herceptin by experimental mammary adenocarcinoma. Nucl Med Rev Cent East Eur 2003;6:99–103.
22. Braun RD, Abbas A, Bukhari SO, Wilson W III. Hemodynamic parameters in blood vessels in choroidal melanoma xenografts and rat choroid. Invest Ophthalmol Vis Sci 2002;43:3045–52.
23. Carraway CA, Carvajal ME, Carraway KL. Association of the Ras to mitogen-activated protein kinase signal transduction pathway with microfilaments. Evidence for a p185(neu)-containing cell surface signal transduction particle linking the mitogenic pathway to a membrane-microfilament association site. J Biol Chem 1999;274:25659–67.
24. Buss F, Arden SD, Lindsay M, Luzio JP, Kendrick-Jones J. Myosin VI isoform localized to clathrin-coated vesicles with a role in clathrin-mediated endocytosis. EMBO J 2001;20:3676–84.
25. Aschenbrenner L, Naccache SN, Hasson T. Uncoated endocytic vesicles require the unconventional myosin, Myo6, for rapid transport through actin barriers. Mol Biol Cell 2004;15:2253–63.
26. Kamal A, Goldstein LS. Connecting vesicle transport to the cytoskeleton. Curr Opin Cell Biol 2000;12:503–8.
27. Mross K, Niemann B, Massing U, et al. Pharmacokinetics of liposomal doxorubicin (TLC-D99; Myocet) in patients with solid tumors: an open-label, single-dose study. Cancer Chemother Pharmacol 2004;54:514–24.
28. O'Brien ME, Wigler N, Inbar M, et al. Reduced cardiotoxicity and comparable efficacy in a phase III trial of pegylated liposomal doxorubicin HCl (CAELYX/Doxil) versus conventional doxorubicin for first-line treatment of metastatic breast cancer. Ann Oncol 2004;15:440–9.
29. Hamaguchi T, Matsumura Y, Nakanishi Y, et al. Antitumor effect of MCC-465, pegylated liposomal doxorubicin tagged with newly developed monoclonal antibody GAH, in colorectal cancer xenografts. Cancer Sci 2004;95:608–13.

In vivo Real-time Tracking of Single Quantum Dots Conjugated with Monoclonal Anti-HER2 Antibody in Tumors of Mice

Hiroshi Tada, Hideo Higuchi, Tomonobu M. Wanatabe, et al.

Cancer Res 2007;67:1138-1144.